Journal of Power Sources, 2 (1977/78) 163 - 176

CURRENT EFFICIENCY IN THE LITHIUM–WATER BATTERY

E. L. LITTAUER, W. R. MOMYER and K. C. TSAI
Lockheed Palo Alto Research Laboratory, Palo Alto, California 94304 (U.S.A.)
(Received March 25, 1977)

Summary

Under well-controlled conditions, the exceptional energy of the Li–H_2O reaction can be harnessed electrochemically with high Faradaic efficiency. The most important adjustable control parameters are electrolyte flow rate, electrolyte concentration, temperature and anode–cathode contact pressure. In single cell discharges, it is simple to control these factors. However, when dealing with multicell battery stacks in a bipolar configuration, good balance from cell to cell is more difficult to attain. This is then reflected by a reduction in efficiency of the Li dissolution reaction. This paper describes a technique to diagnose the efficiency of individual cells or cell stacks via comparison of polarization curves and information on the open circuit corrosion rate of Li in the electrolyte of interest.

Résumé

L'énergie exceptionnellement élevée de la réaction Li–H_2O peut être utilisée avec un haut rendement Faradique. Les plus importantes conditions opératives réglables sont: le débit moyen de l'électrolyte, sa composition, sa température, et la force mécanique entre la cathode et l'anode. Celles-ci sont facilement réglées dans le cas d'une cellule seule. Avec une pile composée de plusieurs cellules un état uniforme pour chaque, nécéssaire afin d'éviter un abaissement d'efficacité de dissolution, est plus difficile à réaliser. Cet article présente les détails d'une méthode qui permet l'observation du rendement des cellules individuelles, ou en groupe, au moyen de courbes de polarisation et de certaines données représentant le taux de consommation de lithium dans l'électrolyte en question sans flux de courant.

Zusammenfassung

Unter gut kontrollierten Bedingungen kann die ausserordentliche Energie der Li–H_2O Reaktion auf elektrochemischen Wege mit hohem Wirkingsgrad ausgenuetzt werden. Die wichtigsten kontrollierbaren Kennummern sind die Fliessgeschwindigkeit der Elektrolyten, die Elektrolytkonzentration, die

Temperatur und der anodisch-kathodischer Kontaktdruck. Zur Entladung einer Einzelzelle sind diese Faktoren leicht zu kontrollieren; aber wenn man mit Ketten von vielen Battarien in bipolarischer Anordnung handelt, ist die Gleichmaessigkeit von Zelle zu Zelle schwerer zu erreichen. Dieses zeigt sich durch Wirksamsgradverminderung der Li Loesungsreaktion. Diese Arbeit beschreibt eine diagnostische Methode zur Bestimmung des Wirksamsgrades der Einzelzellen und der Ketten durch Vergleich der Polarizationskurven mit der Korrosionsgeschwindigkeit des Li im Elektrolyt.

Introduction

Careful cell design is required if maximum electrochemical efficiency is to be attained from Li–H_2O flowing electrolyte primary batteries. Four control parameters profoundly affect battery performance. These parameters are LiOH concentration, electrolyte flow rate across the anode surface, temperature, and because the anode is protected by a porous oxide film, the anode to cathode contact pressure. This latter parameter is important because it has been found that the hydrodynamics within the interelectrode cavity and, by association, the mass transport across the oxide film are critical to anodic behaviour.

When operating single cells, system balance is easily attained and very high electrochemical efficiency is observed. Multicell battery configurations, on the other hand, may present difficulties in equalizing flow rate, LiOH concentration, temperature and contact pressure. A technique is needed therefore to determine the discharge efficiency of each cell in a battery stack by diagnostic analysis of the system's response to changes in the four critical parameters.

Li efficiency determinations generally comprise integrated real-time measurements of the H_2 evolution rate as a function of the current drawn. This technique is effective in determining single-cell or total battery Li efficiencies over a broad range of operational conditions. However, prior to this study it was not possible to determine individual cell efficiencies during battery tests of bipolar stacks which are connected electrically and hydraulically in series. Previously efficiencies were determined via weight measurements of the Li consumed from each anode after a prolonged discharge period.

This paper describes a method which provides a real-time measurement of the average Li utilization efficiency in any multicell battery and, if each cell in the stack has an electrical connection, the individual cell efficiency may also be determined. The only data needed are the slopes of the current–potential curves of the individual cells or the cell stack. These are then compared to base line anodic polarization curves for Li under well-defined operating conditions. The base line curves may be conveniently obtained from a small, single cell, laboratory test apparatus. As will be shown, very close agreement

is obtained between the analytically derived and experimentally measured efficiency values.

Practical details of the Li–H_2O battery system have been given elsewhere [1, 2]. In many ways Li has features similar to other metals which form anodic films in aqueous electrolytes, but in certain cases Li is unique. For example, at a specific potential − 2.66 V (E_H) a transient passivation phenomenon occurs [3] which has not been reported for other metals. On the other hand, like zinc it manifests a characteristic critical current (i_{crit}) and beyond i_{crit} mechanical passivation is observed [4]. Electrolyte flow rate across the anode surface is an important affector of cell performance, and because of unusual properties of the anodic film, anode to cathode contact pressure also influences performance. The ability to electrochemically harness the reactivity of Li in aqueous solution is due exclusively to the properties of this oxide/hydroxide film, which moderates the reaction of the metal with the electrolyte. The film is permeated with electrolyte and it supports high rates of flux with little polarization; in fact, the only measurable polarization at the anode at c.d.'s up to i_{crit} is ohmic. In practice, to optimize Faradaic efficiency, the anode is operated at a c.d. just less than i_{crit}. Another unusual feature of the anodic film is its mechanical strength which is sufficient to allow the cathode structure to be pressed against it at pressure up to 30×10^4 Pa (1 Pa = 1.02×10^{-3} g/cm^2) without causing a short circuit. The cathode comprises a ribbed plate overlayed by a wire mesh screen. Electrolyte flows through the ribs and it passes also through the open volume of the screen adjacent to the film.

Experimental

Single cell tests

Figure 1 gives a view of the cell. The housing was constructed from Plexiglass. It incorporated features to direct electrolyte in a uniform stream between the anode and cathode. The anode comprised a circular 3.8 cm diam. 1.14×10^{-3} m^2, Li disc mounted on a steel back plate. All surfaces other than the active Li face were protected with a stop-off lacquer. The cathode comprised a ribbed steel plate to which was spot-welded a steel mesh screen. The predominant electrolyte flow path is the channel between the screen and the back of the steel plate, but a portion of the flow passes through the screen and washes over the Li surface. Details of an anode and cathode are shown in larger scale in the development battery (Fig. 3).

For most of the single cell tests reported here, one flow rate (0.30 m/s) and one anode to cathode contact pressure setting (6.2×10^4 Pa) was used. The contact pressure was held constant by an air pressure cylinder which incorporated a compensation feature to neutralize the pressure component of the electrolyte flow in the cell. LiOH solution prepared from reagent grade chemicals was circulated from a reservoir, through the cell and back to the reservoir. A heat exchanger was used to maintain electrolyte temperature to within 0.1 °C of the set point 25 °C.

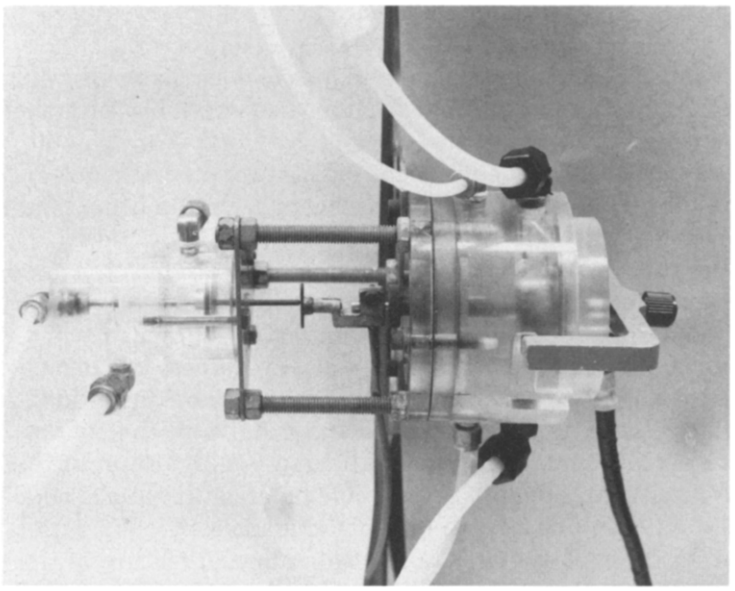

Fig. 1. 1.14 x 10^{-3} m^2 Li–H_2O test cell.

Electrolyte circulation was by a voltage regulated 2 l/min chemically resistant pump in series with a flow meter. With this arrangement the flow rate was controlled to within 0.01 m/s. Flow in the cell was laminar (Re < 400).

Constant load cell polarizations were performed using a carbon pile resistor. Cell voltage and current were monitored with an X–Y recorder. Anode polarization was measured against a $Cd/Cd(OH)_2$ reference probe installed directly adjacent to the anode surface.

The H_2 rate at various polarization levels was measured. In the Li–H_2O system, both the cathodic reduction of H_2O and the direct parasitic reaction of Li with the electrolyte give H_2 as the reaction product. Thus, accurate measurement of the hydrogen evolution rate is necessary. This was accomplished using a wet test meter which was modified by incorporation of a Renco Corporation Model KT23A-500 optical encoder which, when mounted upon the wet test meter shaft, provided a digital signal output of 500 pulses/revolution. The encoder was mounted so that there was no frictional drag component which would amplify inaccuracies at low rate measurements, which are endemic to wet test meters. The output of the encoder was processed by an electronic digital/analog converter which provided instantaneous rate and total gas volume information. The rate of hydrogen evolution was converted from volumetric flow rate (cm^3/s) to current (I) via the ideal gas law and Faraday's law.

Multicell tests

The test stand used for the evaluations of large area lithium anodes is illustrated in Fig. 2. The key components of the system are a battery casing (containing the bipolar cell stack and electrode pressurization system), a liquid–liquid heat exchanger, an electrolyte pump, and a small reservoir which also functions to separate hydrogen from the electrolyte during operation.

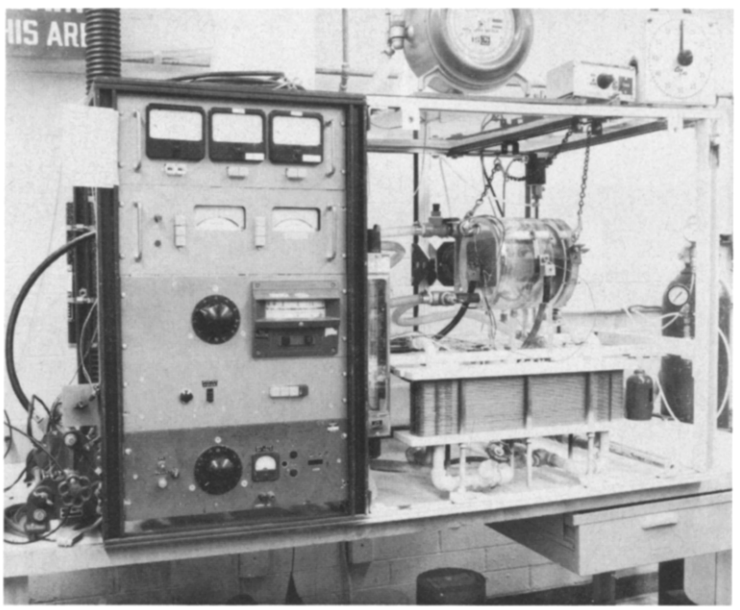

Fig. 2. Battery test stand.

Three battery casing configurations were evaluated in this study; all were fabricated from acrylic plastic to provide visibility during the tests. The same bipolar electrode design was used; however, the electrode manifold channeling was different in each, so as to be able to evaluate the effectiveness of various approaches for both shunt loss reduction and uniformity of electrolyte flow distribution to the individual cells. Typical multicell batteries are shown in Fig. 3. The 5-cell deep ocean battery utilized a large plenum chamber which assured uniform flow distribution. The area of each anode was 415 cm^2 and 4 cm skirts were attached to each bipolar electrode. These skirts provided only a small measure of shunt loss suppression. The 6-cell development battery (165 cm^2 lithium anodes) used a slotted flow tube through the inlet skirt of each electrode to provide both uniform flow and shunt loss reduction. The 10-cell Sonobuoy battery had inlet and outlet slots machined into the sides of the acrylic casing. These slots acted as the electrolyte manifold and

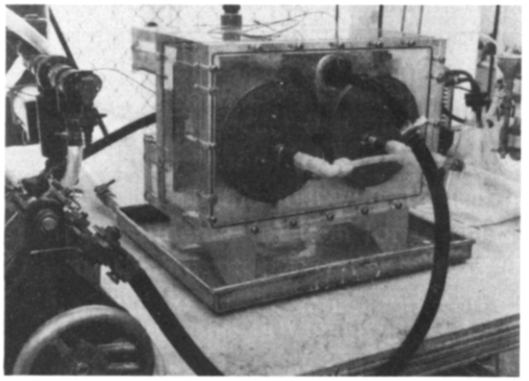

5-CELL PROTOTYPE OF 2 kW, 18 kWh BATTERY FOR DEEP OCEAN APPLICATIONS

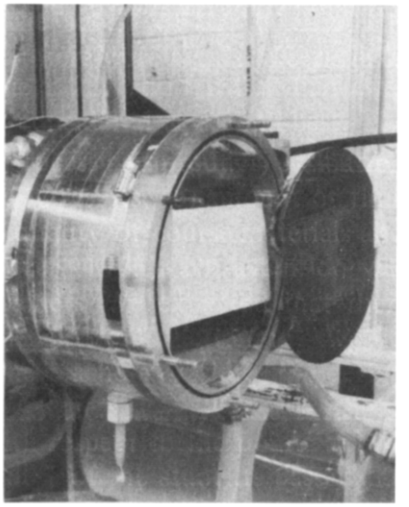

6-CELL 0.25 kW DEVELOPMENT BATTERY

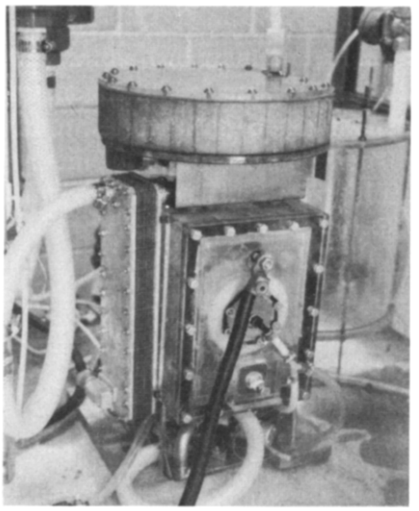

TOTAL SYSTEM. 10-CELL 0.45 kW, 4 kWh BATTERY FOR MARINE APPLICATIONS

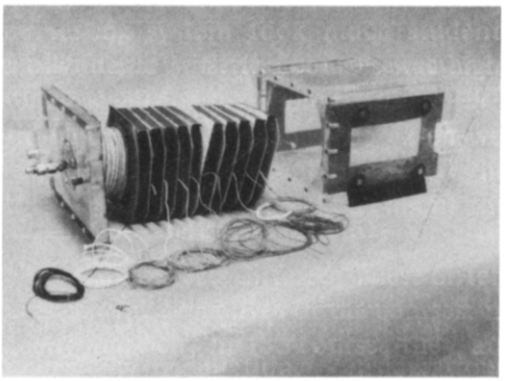

CELL STACK SHOWING BIPOLAR ELECTRODE AND VOLTAGE MONITORING LEADS

Fig. 3. Typical multicell batteries.

provided a high electrical resistance path to help reduce shunt currents. The anodes were 165 cm^2 in area.

Battery power was dissipated in a carbon pile resistor and current was measured across a calibrated 100 mV–100 A shunt. Battery voltage and current were measured with autoranging digital multimeters and recorded on a 2-channel strip chart recorder. Electrical leads were attached to each cell of the deep ocean and development batteries so that individual cell voltages could be measured. Current–voltage curves were displayed with an X–Y recorder. Power output was regulated with an automatic diluent controller,

designed and fabricated in-house. This controller senses battery voltage and admits water into the electrolyte loop through a solenoid valve when the voltage falls below a given set point. Power regulation to ± 1% was achieved with this device.

Lithium current efficiencies were determined both from hydrogen gas evolution rates during a test and gravimetrically at the completion of a test. A specially constructed Ah meter assisted the efficiency determinations. Duration of a test was generally 2 to 8 h to ensure that any weighing error, introduced by changes in the thickness of the lithium hydroxide film on the anode, would be insignificant.

Results

Figure 4 shows selected base line constant load anodic polarization curves. These were obtained in the 1.14×10^{-3} m^2 laboratory test cell using 2.96, 3.94 and 4.84 *M* LiOH. The resistance $R(\Omega/\text{cm}^2)$ of the electrolyte permeated Li oxide film is given by the slope of the linear portion of the *i–E* curves. Table 1 lists *R* for various LiOH solutions.

TABLE 1

Anode film resistance *vs.M* LiOH at 298 K

LiOH (*M*)	$R(\Omega/\text{cm}^2)$
2.96	0.44
3.44	0.66
3.94	1.08
4.6	2.39
4.84	3.43

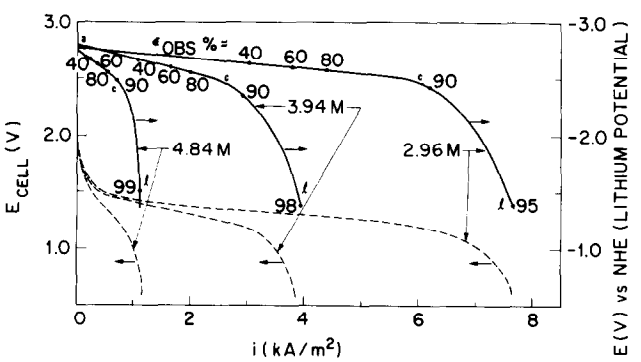

Fig. 4. Anodic polarization of lithium at 298 K in various concentrations of LiOH. Contact pressure = 6.2×10^4 Pa, electrolyte flow velocity = 0.3 m/s. Efficiencies ϵ (%) are shown. The significance of points a, c, *l* is discussed in the text.

Included in Fig. 4 are measured values of the Li current efficiency ϵ_{OBS} at selected points on the polarization curves from open circuit, point a, to point c. Beyond point c concentration polarization and/or mechanical passivation effects significantly degrade cell power output. Point *l* represents the maximum current which can be drawn under the specific test conditions. Also shown in Fig. 4 are the cell polarization curves. The deviation from linearity at low c.d.'s is due to the activation overvoltage for the H_2 evolution reaction (e.r.) on the steel cathode matrix. Figure 5 gives individual cell polarization curves obtained from the 6.25 V, 5-cell deep ocean battery. As was pointed out earlier, attempts were not made with this particular battery design to eliminate shunt power losses and thus, significant intercell currents flow in the common electrolyte. These currents cause the individual cells to polarize even before current is drawn through the external circuit. For this reason, the observed OCV of each cell (1 - 5) is reduced from a typical single cell value of ~ 1.9 V (see Fig. 4) to the 1.5 - 1.6 V in the present case. The major contributor to the internal shunt current polarization effect is the activation overvoltage of H_2 evolution at the cathode. Included in Fig. 5 is the Li anodic polarization plot (curve 6) which was obtained in the laboratory test cell under the overall conditions specified for the 5-cell test. This curve is of course similar to those of Fig. 4. As will be shown in the discussion section, it is used to assess the individual cell efficiencies shown as ϵ_{CALC} in the Figure. The gravimetrically measured Li energy density (3500 Wh/kg Li) which is equivalent to 72.5%, compares well with the calculated average efficiency of the 5 cells which is 71.8%.

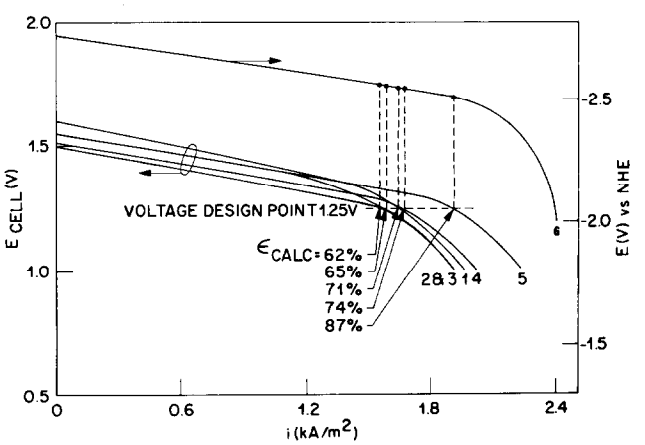

Fig. 5. Individual cell voltages (1 - 5) *vs* current density in 3.64 *M* LiOH at 291 K. Electrolyte flow velocity = 0.21 m/s, contact pressure = 6.9 × 10^4 Pa. Curve 6 shows anodic polarization of Li under identical conditions. Calculated Li efficiencies for cells 1 - 5 are shown.

Results obtained with the 6-cell development battery are shown in Fig. 6. This unit, with its high resistance slotted flow tube, demonstrated significantly

reduced shunt current losses on the inlet side of the cell stack. Plots 1 - 6 show each cell's i–E curve, plot 7 gives the base line anodic polarization obtained in the laboratory test cell. Calculated efficiencies ϵ_{CALC} and the observed values ϵ_{OBS} are given.

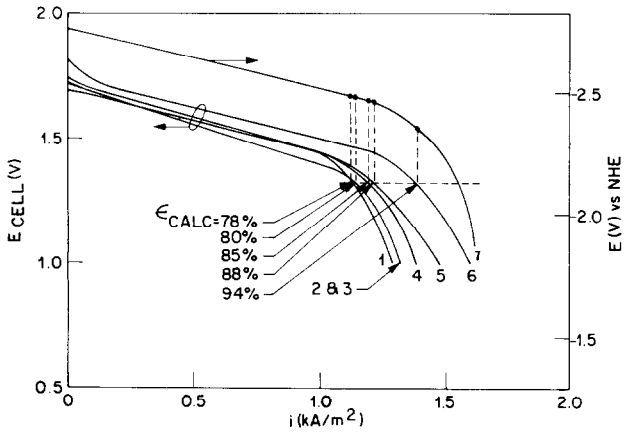

Fig. 6. Individual cell performance of 6-cell Li–H_2O battery in 4.2 M LiOH at 296 K. Electrolyte flow velocity = 0.15 m/s, contact pressure = 4.9 x 10^4 Pa.

Figure 7 indicates the polarization and efficiency features of the 10-cell, 12.5 V Sonobuoy battery. This unit was equipped with advanced shunt suppression features. Accordingly, its 18 V OCV is depressed by only 1 V from the sum of the single cell potentials (1.9 V). Included are the calculated aggregate cell stack efficiencies ϵ_{CALC} and the observed efficiencies ϵ_{OBS} under the conditions shown at the battery design voltage (12.5 V).

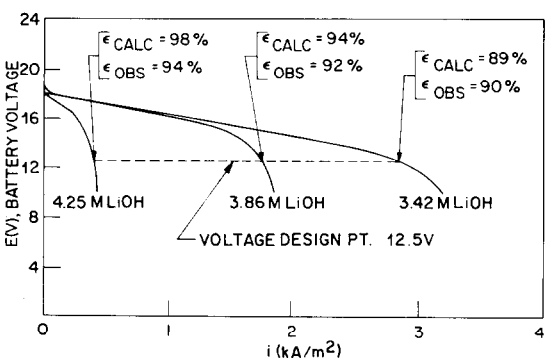

Fig. 7. Polarization characteristics of 12.5 V Sonobuoy battery at three power levels: 80 W, 360 W and 600 W. Gravimetrically measured Li utilization efficiency (ϵ_{OBS}) compares with calculated aggregate values (ϵ_{CALC}).

Discussion

The anodic dissolution of Li comprises two competitive processes, *i.e.*, electrochemical and parasitic processes as described by the following equations:

$$\text{electrochemical reaction: } Li + OH^- \rightarrow LiOH + e \quad (1)$$

$$\text{parasitic reaction: } Li + H_2O \rightarrow LiOH + 1/2H_2 \quad (2)$$

Typical anodic polarization curves are shown in Fig. 4. Between OCV point a, and the polarization level corresponding to point c, a combination of (1) and (2) occurs. At higher polarization levels, depicted as region c–*l*, reaction (1) predominates. In the straight line region a–c, it is reasonable to postulate that the polarization is mostly ohmic and the i_e–E relationship can then be expressed simply by:

$$\eta = i_e A R \quad (3)$$

where η is the anode overvoltage ($E_a - E'_0$), i_e is the electrochemical current density, A is the projected surface area, R is the resistance across the anodic film. Reaction (2) can be regarded as a combination of two local cell reactions, *i.e.*,

$$Li + OH^- \rightarrow LiOH + e \quad (2a)$$

$$H_2O + e \rightarrow OH^- + 1/2H_2 \quad (2b)$$

and, as has recently been shown [5], the cathodic evolution of H_2 on the oxide-filmed Li anode is rate determining — the transfer coefficient α has a value of 0.14.

The current density (i_p) *vs.* cathodic overvoltage (η_c) curves can be described by the Tafel relationship (when $\eta_c > 50$ mV):

$$\eta_c = a + b \log i_p \quad (4)$$

where i_p is the parasitic corrosion rate, *i.e.*, the H_2 evolution rate per apparent unit area of Li surface and a, b are constants. The Tafel slope $b = RT/n\alpha F$, then since $n = 1$ and $T = 298$ K, for the H_2 e.r. on Li, the slope $b = 416$ mV/decade.

At OCV the overvoltage for the H_2 e.r. at the active Li electrode is very high, *i.e.*, $\eta_c = +1.93$ V. Curves A and C in Fig. 8 show illustratively the two local cell reactions described by eqns. (2a) and (2b). E_c represents the measured OCV of Li *vs.* NHE. E_H(-0.84 V) denotes the equilibrium potential of the H_2 e.r. at pH = 14, and E_{Li} is the equilibrium potential for the charge transfer reaction of Li. Curve B in Fig. 8 represents the mixed potential of the two reactions.

Rewriting eqn. (4), we have:

$$i_p = i_0 \exp\left(\frac{\alpha F}{RT}\eta_c\right) \quad (5)$$

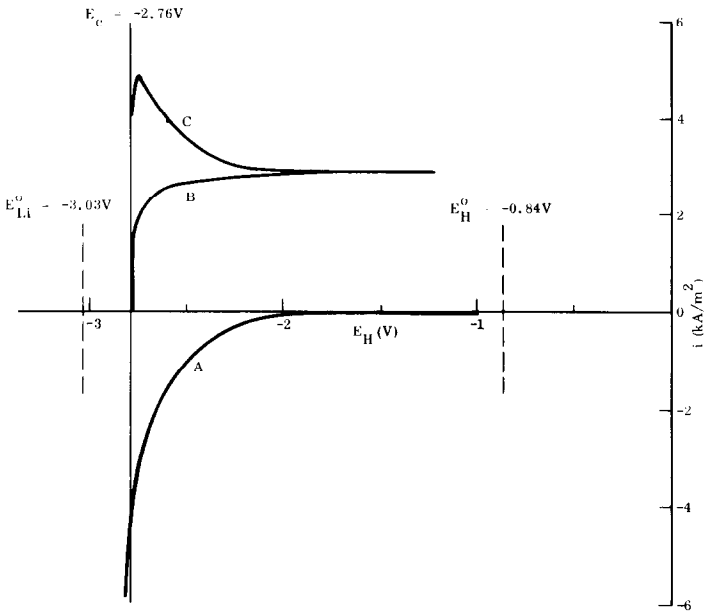

Fig. 8. Composite diagram showing hydrogen evolution polarization plot on Li (A), actual mixed potential polarization plot for Li (B) and generated anodic dissolution plot of Li (C) in 4.1 *M* LiOH at 298 K.

where i_0 is the apparent exchange current density for the H_2 e.r. on the Li surface, F, R, T have their usual significance.

$$\eta_c = -E_a + E_H$$
$$= -(E'_0 - E_H) - \eta \qquad (6)$$

where E_a is the potential of the Li electrode at a given c.d. and η is the total anodic overvoltage of the Li. At OCV, $\eta = 0$ and thus $\eta_c = -(E'_0 - E_H) =$ 1.93 V. Equation (5) can be simplified:

$$i_p = \upsilon \exp\left(-\frac{\alpha F}{RT}\,\eta\right) \qquad (7)$$

in which $\upsilon = i_0 \exp\left[-\frac{\alpha F}{RT}(E'_0 - E_H)\right]$

and is equivalent to the reaction rate for (2b) at the Li electrode, *i.e.*, the OCV corrosion c.d.

The current efficiency, ϵ, at the anode is defined by:

$$\epsilon(\%) = \frac{|i_e|}{|i_e| + |i_p|} \qquad (8)$$

Then substituting eqn. (3) for i_e and eqn. (7) for i_p into eqn. (8), we have:

$$\epsilon(\%) = \frac{\eta/AR}{\eta/AR + \upsilon \exp\left(-\frac{\alpha F}{RT}\eta\right)}$$

and dividing:

$$\epsilon(\%) = 1 - \frac{AR}{\eta}\upsilon \exp\left(-\frac{\alpha F}{RT}\right) + \left(\frac{AR}{\eta}\right)^2 \upsilon^2 \exp\left(-\frac{2\alpha F}{RT}\eta\right) - \left(\frac{AR}{\eta}\right)^3 \times$$

$$\upsilon^3 \exp\left(-\frac{3\alpha F}{RT}\eta\right) + \cdots\cdots$$

which can be expressed by the summation term:

$$\epsilon(\%) = \sum_{m=0}^{\infty} (-1)^m \upsilon^m \left(\frac{AR}{\eta}\right)^m \exp\left(-\frac{m\alpha F}{RT}\eta\right) \tag{9}$$

where m is an integer. All the terms needed to solve eqn. (9) have been accounted for other than υ the reaction rate for the H_2 e.r. on the Li at OCV. This may be obtained experimentally from a measurement of the OCV Li corrosion rate, *i.e.*, the H_2 evolution rate under the specified conditions or it can be calculated*.

Thus, using eqn. (9) it is, in principle, possible to generate a complete plot of current efficiency *vs.* polarization. To do this requires that a large number of integers be used and the mathematical solution would be cumbersome. In the present investigation, Li efficiencies at polarization fairly close to the critical current are the ones of greatest interest. Here, the anode polarization will be condiderably greater than 100 mV (η at i_c (i_{crit}) ranges from 270 to 330 mV). It has been found that if the integer, m, is set at 10, a simple treatment will handle the 11 term series calculation to give acceptable data. This can be seen when calculated υ values from eqn. (10) and experimental R values are inserted in eqn. (9) to generate curves of ϵ% *vs.* i in 4.84, 3.94, and 2.96 M LiOH. These are displayed as the solid lines in Fig. 9. In this Figure, actual measured current efficiencies where $\epsilon(\%)$ = equivalent H_2 evolution rate for a given i divided by the rate of total H_2 evolution, are plotted against i and are represented by broken lines. A comparison of the curves obtained experimentally and analytically shows how well the analytical expresison for $\epsilon(\%)$ agrees with actual cell operation data. Applications

---

*In a previous paper [5] which dealt with the corrosion of Li in LiOH solution, an empirical equation was derived from which the corrosion rate at OCV, i_{corr}, can be calculated for any temperature (up to about 333 K) over the range of LiOH concentration used in Li–H_2O cells.

$$i_{corr} = (54.1 - 10[\text{LiOH}]) \exp\left(25.04 - \frac{7.84 \times 10^3}{T}\right)$$

and

$$i_{corr}(\text{kA/m}^2) = \upsilon \tag{10}$$

(The activity of Li is assumed to be unity.)

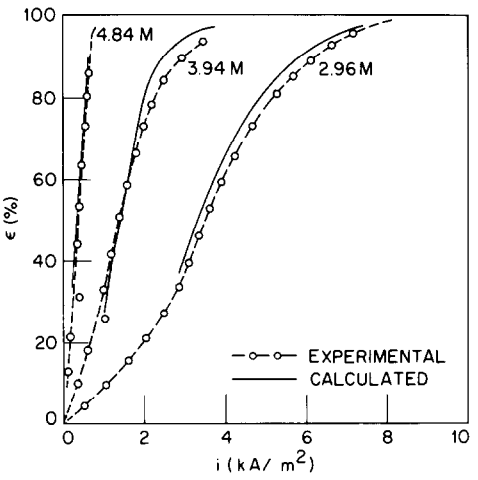

Fig. 9. Current efficiency of Li in Li–H_2O cell at various LiOH concentrations.

of the model to assessment of multicell performance is now illustrated for the case of the 5-cell, 6.25 V deep ocean battery. Figure 5 gives individual cell polarization curves (1 - 5) and the Li anodic polarization curve (6). It is apparent that at the operating cell voltage (1.25 V) each cell was discharging at a somewhat different c.d. As examples, cell 1 was at 1.6 kA/m^2 and cell 5 at 1.92 kA/m^2. The slope of the linear portion of curve 6 gives its resistance R(1.35 Ω/cm^2) and the OCV corrosion rate, υ, was calculated to be 2.64 kA/m^2 in the 3.64 M LiOH solution at 18 °C. Also, from eqn. (3), $\eta = i_e AR$, then η at cell 1 (i = 1.6 kA/m^2) and at cell 5 (i = 1.92 kA/m^2) can be calculated.

All the data now exist for insertion into eqn. (9) and computing the series gives the current efficiencies indicated as $\epsilon(\%)_{CALC}$. The average of 71.8% compares closely with that obtained gravimetrically (72.5%) after an 8 h run. The performance features of the 6-cell development battery are shown in Fig. 6. By wiring each cell, it is possible to introduce subtle changes into the system and the impact of such changes is immediately reflected by the individual efficiency diagnosis. When the system operating parameters are finally optimized, it is only necessary to run whole stack polarizations as shown in Fig. 7 to verify that battery performance meets specifications. In any Li–H_2O multicell system, other than for the parasitic reaction current, the internal shunt currents also degrade the anodic current efficiency. Therefore, it will be noted when comparing Fig. 9 with Figs. 6, 7 and 8, the average multicell current efficiency is always less than that of a single cell. Equation (9) serves to effectively calculate the current efficiency in multicell and single cell systems.

Conclusion

The anodic polarization of lithium in aqueous electrolytes is predominated by the ohmic drop across its porous oxide films. This ohmic polarization

feature allows the derivation of a diagnostic empirical equation for the calculation of current efficiency. This is critical to the operation of Li–H_2O cells. Thus by merely knowing the ohmic resistance of the film and the parasitic reaction rate at OCV, the current efficiency can be calculated at any given current density. These calculated current efficiencies have been tested against experimentally measured data and found to be in good agreement. An important feature of this derived equation is that it requires no knowledge of the internal shunt currents in a multicell system since these currents only impact on the current inefficiency of the individual cells. The empirical equation also permits calculation of individual anode current efficiencies which cannot be measured directly in bipolar multicell stacks.

References

1 H. J. Halberstadt, E. L. Littauer and E. S. Schaller, Rec. Tenth Intersoc. Energy Convers. Eng. Conf., Newark, Del., 1975, 1120 - 1125.
2 D. D. Kemp, E. L. Littauer, W. R. Momyer and J. J. Redlien, Proc. Eleventh Intersoc. Energy Convers. Eng. Conf., Lake Tahoe, Calif., Sept., 1976, 462 - 466.
3 E. L. Littauer and K. C. Tsai, J. Electrochem. Soc., 123 (6) (1976) 771.
4 E. L. Littauer and K. C. Tsai, J. Electrochem. Soc., 123 (7) (1976) 964.
5 E. L. Littauer and K. C. Tsai, J. Electrochem. Soc., 124 (6) (1977) 851.